Received: 20 April 2021 | Revised: 16 November 2021 | Accepted: 17 November 2021

DOI: 10.1002/mrm.29113

RESEARCH ARTICLE

Magnetic Resonance in Medicine

T_2 quantification in brain using 3D fast spin-echo imaging with long echo trains

Jeff Snyder[1] | **Kelly C. McPhee**[2] | **Alan H. Wilman**[1]

[1]Department of Biomedical Engineering, University of Alberta, Edmonton, Canada

[2]CancerCare Manitoba, Winnipeg, Canada

Correspondence
Jeff Snyder, Department of Biomedical Engineering, University of Alberta, 1098 Research Transition Facility, Edmonton, Alberta, T6G 2V2, Canada.
Email: jeff.snyder@ualberta.ca

Funding information
Natural Sciences and Engineering Research Council of Canada, Grant/Award Number: RGPIN-2017-04006; Canadian Institutes of Health Research, Grant/Award Number: MOP 102582

Abstract

Purpose: Three-dimensional fast spin-echo (FSE) sequences commonly use very long echo trains (>64 echoes) and severely reduced refocusing angles. They are increasingly used in brain exams due to high, isotropic resolution and reasonable scan time when using long trains and short interecho spacing. In this study, T_2 quantification in 3D FSE is investigated to achieve increased resolution when comparing with established 2D (proton-density dual-echo and multi-echo spin-echo) methods.

Methods: The FSE sequence design was explored to use long echo trains while minimizing T_2 fitting error and maintaining typical proton density and T_2-weighted contrasts. Constant and variable flip angle trains were investigated using extended phase graph and Bloch equation simulations. Optimized parameters were analyzed in phantom experiments and validated in vivo in comparison to 2D methods for eight regions of interest in brain, including deep gray-matter structures and white-matter tracts.

Results: Phantom and healthy in vivo brain T_2 measurements showed that optimized variable echo-train 3D FSE performs similarly to previous 2D methods, while achieving three-fold-higher slice resolution, evident visually in the 3D T_2 maps. Optimization resulted in better T_2 fitting and compared well with standard multi-echo spin echo (within the 8-ms confidence limits defined based on Bland-Altman analysis).

Conclusion: T_2 mapping using 3D FSE with long echo trains and variable refocusing angles provides T_2 accuracy in agreement with 2D methods with additional high-resolution benefits, allowing isotropic views while avoiding incidental magnetization transfer effects. Consequently, optimized 3D sequences should be considered when choosing T_2 mapping methods for high anatomic detail.

KEYWORDS
extended phase graph, fast spin echo, quantitative MRI, relaxation, T_2

1 | INTRODUCTION

Three-dimensional spin echo (SE)–based methods are gaining a significant foothold in weighted imaging and can provide increased resolution often with only negligible effects to total imaging time.[1–3] In terms of 3D turbo spin echo or fast spin echo (FSE), optimized long echo trains[4–11] in combination with short interecho spacings and low refocusing angles has resulted in specialized sequences delivering T_1, T_2, or proton-density (PD) contrast while minimizing acquisition time (TA) and specific absorption rate. These methods have different names depending on manufacturer, such as SPACE (Sampling Perfection with Application optimized Contrasts using different flip angle Evolution [Siemens]), CUBE (General Electric), and VISTA (Volume Isotropic Turbo spin echo Acquisition [Philips]).

Although increased use of 3D-weighted imaging is emerging, it still lacks the robust, clinical quantification options widely developed for the 2D-FSE analogue. The two prominent 2D methods include acquiring several echoes along the signal decay curve (multi-echo spin-echo [MESE]) or dual-echo (PD-T2) approaches. Although MESE is considered the gold standard for T_2 mapping, it is time-consuming and generally not clinically available. As shown in McPhee and Wilman,[12] dual-echo FSE T_2 mapping from PD and T_2-weighted contrasts can be accurate if the spin response and flip angles are properly modeled. With adequate SNR, PD-T2 methods have shown to produce similar results to MESE for a specified range of T_2 values, while substantially shortening imaging time due to acquisition of only two effective TEs. Modeling the PD-T2 approximation to the decay curve requires inclusion of the measured flip angles (i.e., the deviation of flip angle from nominal) through B_1^+ map generation[13] and detailed knowledge of the pulse sequence. Improving resolution is possible due to decreased TA over MESE, although 2D sequences generally have lower resolution in the slice direction than in-plane, which may result in partial voluming and misclassification of T_2s. The 2D PD-T2 methods can also be confounded with incidental magnetization-transfer effects.[14] These drawbacks are considerable, although 2D T_2 mapping is well established and used in clinical studies.

Building on the 2D approach to T_2 fitting, 3D methods have become viable due to sequence modifications, allowing shortening of the TA by using long FSE trains with low flip angles and short interecho spacing, obtaining multiple subresolution images at several TEs, or the addition of gradient-echo (GE) modules to speed data acquisition. Subresolution images, such as those acquired in the stack of stars technique,[15,16] use long echo trains, optimized flip angles, and subspace reconstruction methods to extract T_2 information for each echo, thereby decreasing the total TA from a dual-echo or multi-echo scheme, with the drawback of producing a single weighted image for a specific TE. Combination GE/SE techniques speed up the acquisition by additional GE modules following SE trains[17] or interleaving of SE and GE acquisitions, such as typically used in myelin-water mapping methods.[18] T_2-preparation pulses can also be used in standard 3D-SE sequences to produce different magnetization pathways,[19] resulting in T_2 mapping ability but limited to single image output. Furthermore, the development of specialized MR fingerprinting sequences[20–23] has pushed quantification boundaries while seeking to maintain resolution with clinical images within relatively short TAs.

Given the multiple techniques available, T_2 quantification from 3D FSE appears promising, although specialized research sequences unavailable in the clinic are often used. Constraining techniques to clinical sequences, the comparison of 3D FSE (often used for high-resolution anatomical images such as fluid-attenuated inversion recovery and T_2-weighted and T_1-weighted contrast) with established 2D methods is required to prove clinical utility and accuracy. Three-dimensional FSE differs from 2D primarily in the use of extremely low and variable refocusing flip angles and long echo trains, which has not been fully investigated for T_2 fitting as compared with gold-standard 2D methods.

In this work, we explore T_2 quantification from long echo train 3D-FSE sequences using PD-weighted and T_2-weighted acquisitions with optimized echo train parameters, while keeping resulting standard-weighted PD and T_2 images. This allows a direct comparison between the established 2D PD-T2 method, as both rely on properly fitting the signal acquired from imaging data at different time points to a set of predicted values (a simulated MR sequence dictionary).[24] An easy-to-visualize example—similar to 2D—of a constant flip angle train is used as the initial starting point, and more complicated examples using variable flip angle trains are later examined in simulation, phantom, and healthy volunteer brain experiments.

2 | METHODS

To quantify the performance of 3D-FSE sequences for T_2 mapping, simulations are necessary to provide dictionary values for both decay curve matching and improved fitting via parameter optimization. Although the optimization and evaluation approach is presented for the generic case, the solution space is systematically constrained to two types of sequences, specifically the constant flip angle train mimicking 2D acquisitions and a common T_2-weighted variable flip angle train. Once the sequence has

been analyzed, phantom and volunteer experiments were conducted to verify the numerical outcomes.

2.1 | Choosing a 3D-FSE sequence

The first step is to choose a desired 3D-FSE sequence to determine T_2 mapping performance. Common sequences include constant flip angle trains or scanner-defined variable flip angle trains targeting specific image weightings (PD-weighted, T_2-weighted, or T_1-weighted). Knowledge of the echo train length (ETL), echo spacing, TR, and flip angle array is required for sequence evaluation.

2.2 | Pulse sequence simulations

The a priori information required for quantification, the decay curve dictionary, can be as simple as assuming a mono-exponential decay and fitting the acquired image points, although studies have shown that this approach results in heavily biased T_2 values. Accurate T_2 quantification requires true sequence simulation using extended phase graph (EPG[25] for 3D) or Bloch equation techniques (2D and 3D) to account for indirect and stimulated echoes when flip angles deviate from 180°.[26,27] Furthermore, in 2D experiments, slice selection and crusher gradient application requires simulation of spins in space.[26,28,29] Additionally, while simulations can predict the response at each echo for a fully relaxed system, steady-state solutions should be explored when using TRs shorter than complete relaxation described by typical in vivo longitudinal relaxation rates.

Fortunately, 3D FSE often uses nonselective refocusing; therefore, slice modeling is not required, resulting in significant overhead time savings. Instead, single voxels can be modeled as receiving a constant B_1^+ rather than a slice profile distribution. The simplest and most intuitive FSE sequence uses a reduced (from 180°) constant refocusing flip angle throughout the echo train, with a series of intermediate pulses following the 90° excitation pulse to move the response into the pseudo-steady state (PSS).[30,31] More generic sequences manipulate the flip angle evolution in terms of plateaus and ramps to provide increased signal sustainability at a certain level, reduction of point-spread function artifact, or selection of specific mixed contrasts through traversal of the k-space center at a specific TE with optimized signal.[10] As discussed in Weigel and Hennig,[5] the flip angle evolution for FSE can be described by several sections, consisting of a transition from excitation to the PSS, a flip angle ramp, and a plateau followed by a transition to a second PSS. During the ramp, flip angles are increased for succeeding echoes to generate a relatively high signal plateau for k-space center acquisition (for examples, see Mugler[10]).

For each echo train investigated, simulations of decay curves were produced using in-house MATLAB code, modeling steady-state nonselective EPG and Bloch equation solutions for various combinations of T_1, T_2, and B_1^+, with other sequence parameters fixed (ETL, echo spacing, TR, and flip angle array). The decay curve dictionary is therefore a 4D matrix with dimensions of T_1, B_1^+, T_2, and echo number (or TE). After the dictionary is constructed, fitting involves matching image points (PD, T_2, and B_1^+) to simulated decay curves, with the assumption that T_1 does not vary significantly (see Section 3).

2.3 | Echo-time selection

The fitting approach requires selection of TEs for two images, to model the simulated decay curve and provide T_2 quantification. Curve fitting will be successful if there is (1) sufficient SNR for both echoes to alleviate T_2 errors from noise,[12] and (2) adequate variance in relative signal intensity between PD and T_2 across the T_2 range of interest. Although actual image weighting may differ based on TE selection, S_1 and S_2 will refer to the signal of the PD and T_2 images, respectively. These two requirements can be explored using calculated signal parameters. First, the difference between the two echo signals, $S_d = S_1 - S_2$, can be used as a measure of available contrast. A large range of S_d values across the T_2 range of interest is desirable to allow maximum distinction between T_2 isochromats. In other words, S_d should be as large as possible for each investigated T_2 value, and S_d should also be different for each T_2 value in the range of interest to prevent multiple fitting solutions. As S_d will depend on sequence parameters, parameter maps provide insight into the variation of S_d and performance across the T_2 range (e.g., S_d as a function of T_1 and T_2). To aid TE selection for the two images for an individual sequence, a normalized difference parameter, S_{nd}, can be defined as

$$S_{nd} = \frac{S_1 - S_2}{S_1} = 1 - \frac{S_2}{S_1}, \tag{1}$$

ensuring that each difference is weighted by the signal of the first echo. For a typical decay, S_2 is less than S_1 (e.g., during a near-exponential decay) and therefore $0 \le S_{\mathrm{nd}} \le 1$. In the case when a later echo (S_2) has greater amplitude than S_1, a negative value for S_{nd} occurs (signal ramp). During a perfect plateau in the signal, $S_1 = S_2$ and $S_{\mathrm{nd}} = 0$. S_{nd} is a means for measuring the difference produced by the sequence for individual T_2s to be mapped, and due to the normalization, this parameter can be compared between different sequences. To include both parameters (S_d and S_{nd}) in measuring the T_2

mapping performance of a sequence, a third measure can be constructed as follows:

$$S_p = S_d \cdot S_{\mathrm{nd}}. \tag{2}$$

The S_p parameter essentially weights the differences in T_2 mapping values (S_{nd}) by the available contrast (S_d) based on the difference of the two points.

As S_p depends on specific selections of TEs for evaluation, a method is needed to determine optimal TEs for the PD and T_2 images. An iterative scheme can be used by looping through all echoes in the train and computing S_{nd} for each pair of echoes. By fixing T_1 and B_1^+ and constraining T_2 to in vivo values, a matrix of modified S_{nd} values (oT2) can be computed with dimensions ETL × ETL, and each element described by

$$\begin{aligned} \mathrm{oT2}_{i,j}(B_1^+, T_1, T_2) &= S_{\mathrm{nd}}(T_{2\,\max})_{i,j} - S_{\mathrm{nd}}(T_{2\,\min})_{i,j}, \\ \mathrm{oT2}_{i,j} &= 1 - \frac{S_i(T_{2\,\max})}{S_j(T_{2\,\max})} - \left(1 - \frac{S_i(T_{2\,\min})}{S_j(T_{2\,\min})}\right), \\ \mathrm{oT2}_{i,j} &= 2 - \frac{S_i(T_{2\,\max})}{S_j(T_{2\,\max})} + \frac{S_i(T_{2\,\min})}{S_j(T_{2\,\min})}. \end{aligned} \tag{3}$$

where S is the signal for the ith or jth echo, and $T_{2\,\max}$ and $T_{2\,\min}$ represent the maximum and minimum T_2s to be investigated. Consequently, each oT2 value describes the signal variation between extreme values in the T_2 range (i.e., the spread between $T_{2\,\min}$ and $T_{2\,\max}$), with the largest oT2 value corresponding to the echo combination producing the maximum signal variation between T_2s.

As an example to visualize the signal parameters, consider the plot in Figure 1E illustrating S_{nd} for a range of T_1 and T_2 values for the constant 32-echo case, with echo selections of 1 and 16. In healthy brain samples in vivo at 3 T, expected values of T_2 and T_1 fall in the range of 40–90 ms and 800–1400 ms,[32] respectively. A single point in the oT2 matrix (i.e., the available mapping space for T_2 values at echoes 1 and 16) can be estimated using S_{nd} and taking the difference of S_{nd} (B_1^+, T_1, 0.1 s) and S_{nd} (B_1^+, T_1, 0.03 s), where B_1^+ and T_1 are the constant values used for subtraction in Equation (3) and the T_2 range has been broadened to allow for uncertainty. Note that in sequences with strong T_1 dependence, this approximation will not hold, as different T_1s will produce different results. To complete oT2 generation, the difference calculation is repeated for each combination of echo pairs ranging from 1 to ETL. Optimal TEs are then chosen based on the maximum value of oT2. After TE selection is determined for a given sequence, it is important to consider the signal parameters: the total signal difference between echoes reflecting SNR

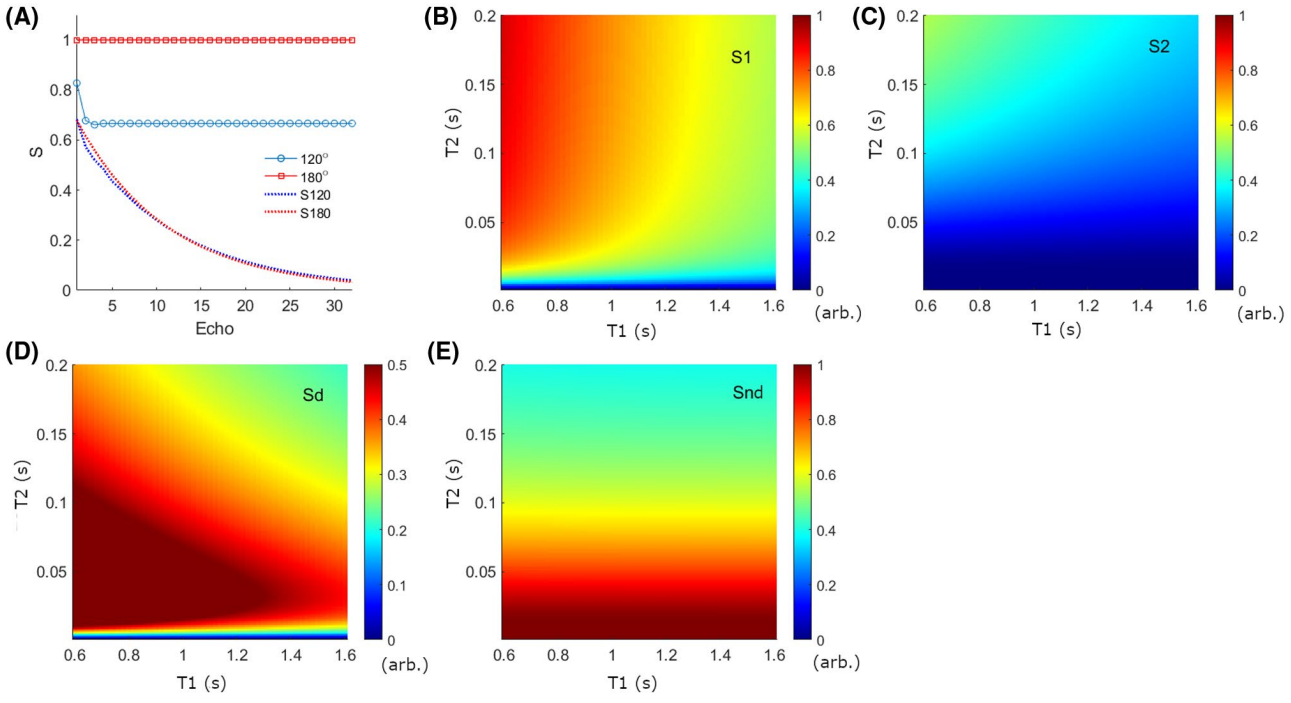

FIGURE 1 Echo signal, signal difference (S_d), and normalized difference (S_{nd}) as a function of T_1 and T_2 with $B_1^+ = 1.0$ for a 32-echo constant flip angle train. (A) Comparison of flip angles and responses (S120 and S180) between the constant 120° (circles) and 180° (squares) trains for $T_2 = 100$ ms and $T_1 = 1$ s (flip angles are normalized to 180°). Signal amplitudes are shown for echo 1 ($\mathrm{TE_{eff}} = 6$ ms) (B) and echo 16 ($\mathrm{TE_{eff}} = 96$ ms) (C). The signal has been normalized to the maximum achievable value of 1.0 at TE = 0. (D) S_d parameter, and (E) Normalized differences (S_{nd}). Note that the nearly horizontal contours in S_{nd} reflect the T_1 invariance (TR = 1.4 s).

(S_d) and the normalized difference showing T_2 decay spread and T_1 dependence (S_{nd}), which are reflected in S_p. Additionally, images should be visually inspected to ensure that the desired contrast is produced for the PD-weighted and T_2-weighted images to maintain clinical usability. Once S_p has been computed, different sequences can be compared at optimal TEs.

2.4 | Steps for sequence evaluation

In summary, optimization of the sequence includes the following steps:

1. Choose a flip angle evolution either manually or based on clinical implementations of 3D FSE sequences with a specified flip angle array, ETL, TR, and echo spacing.
2. Simulate the sequence (in T_1, T_2, and B_1^+ space) using Bloch equation or EPG simulations to produce a dictionary of signal-decay values.
3. Compute oT2 and determine the optimal TEs (using oT2 and visually inspecting contrast) for the PD (S_1) and T_2 (S_2) images.
4. Calculate S_d, S_{nd}, and the combined parameter, S_p, using the optimal TEs from oT2 and validate the constant T_1 approximation (using 3D plots of S_{nd} in T_2 and T_1 space).
5. Determine S_p response across T_2s of interest (using 3D plots of S_p in T_2 and T_1 space).
6. Repeat steps 1–5 for different sequences to evaluate different flip angle evolutions on T_2 mapping and compare S_p.

Selection optimization will be discussed in examples given in the following sections.

2.5 | Constant echo train

Simulations were conducted to model echo trains with ETLs of 16 (the 3D analogue of the 2D PD-T2 FSE sequence) and 32. Contrast is typically reflective of PD-weighted and T_2-weighted images, with degree dependent on the selected echoes, similarly to 2D PD-T2 methods. Therefore, the first echo in the train was chosen for S_1, and a middle echo was used for S_2. Constant cases used flip angle trains with PSS initialization through a one-ahead approach described in Hennig et al.[4] The signal difference, S_d, was calculated across T_1, T_2 and B_1^+, and while S_{nd} can still be used to help understand the constant case, its utility is greater in more complex trains.

2.6 | Generic echo trains

A 96 ETL with variable refocusing angles using the PSS-ramp-plateau-ramp flip angle approach described earlier was investigated. Generally, this shape is used for T_2-weighted contrast in 3D-FSE images and sustains relatively high signal at later TEs. (For example, the T_2-weighted variable flip angle train for our Siemens Prisma produces a plateau for the $T_2 \sim 100$ ms species.) The signal plateau was varied between responses for $T_2 = 50$ (P50), 100 (P100), and 200 (P200) ms species to investigate the T_2 spread based on S_p. Echo-time selection was performed through oT2 optimization.

2.7 | B_1^+ analysis

As B_1^+ is also a variable used in the fitting, S_{nd} can be computed for expected B_1^+ ranges (S_{nd} [B_1^+]), given the optimized TEs for each sequence to evaluate the variation of T_2 fitting response in terms of B_1^+ and ensure that a large signal difference is present to provide unique mapping solutions. For T_2 values of 20–100 ms, B_1^+ ranging from 0.7 to 1.25, and a constant $T_1 = 1$ s, signal parameters S_d, S_{nd}, and S_p were computed. Additionally, experiments were performed on a doped spherical phantom to measure P200 T_2 mapping performance in varying B_1^+ environments, detailed in the next section.

2.8 | Phantom and healthy brain experiments

All data were acquired using a Siemens Prisma (Erlangen, Germany) 3 T scanner with an 80 mT/m gradient set. A Siemens 64-channel head and neck array was used for signal reception. The phantom consisted of six 50 mL tubes filled with water and doped with magnesium chloride to simulate different T_2 environments ranging from 40 to 82 ms (with T_1 ranging from 720 to 1950 ms). Sequences tested included 2D MESE, 2D PD-T2, C32 (constant flip angle 32-echo train), C16, P200, P100, and P50 (acquisition parameters detailed subsequently). Experiments using an additional spherical phantom (20 cm diameter, doped with 1.25 g $NiSO_4$/L) were conducted to measure the T_2 mapping performance of P200 in an environment mimicking the B_1^+ variation in the human head.

The volunteer study consisted of 3 healthy subjects giving informed consent with ages of 23, 30, and 42 years. Parameters for 3D-FSE quantification included two independent experiments with optimized TEs (P200: 54 and 294 ms; P100: 78 and 318 ms; P50: 60 and 198 ms;

C32: 6 and 96 ms), TR = 1.4 s, an isotropic resolution of 1 mm^3 (matrix size of 256 × 256 × 208), parallel imaging (GRAPPA) with an acceleration factor of 2 in the phase-encode dimension, echo spacing of 6 ms, and a TA depending on ETL (96 for P200, P100 and P50; and 32 for C32). A B_1^+-mapping sequence using the Bloch-Siegert[33] method was included to supply flip angles to the quantification, with parameters of TE = 2.24 ms, TR = 4.6 ms, flip angle = 5°, voxel size = 1.1 × 1.1 × 3.0 mm^3, matrix size = 192 × 192 × 36, and TA = 33 s. Furthermore, an MP-RAGE sequence (1 mm^3 isotropic, TE = 2.27 ms, TI = 1800 ms) was used as reference for registering all images using FSL FLIRT.[34–36] Finally, compared with previous 2D methods, standard 2D PD-T2 (16 ETL, TE_1 = 10 ms, TE_2 = 90 ms, 10-ms echo spacing, TR = 7000 ms, flip angle [constant] = 165°, 1.0 × 1.0 mm^2 in-plane resolution with 3-mm slices [35 total], TA = 3:58 min) and 2D MESE images (32 ETL, 10-ms echo spacing, TR = 3000 ms, flip angle = 180°, 1.0 × 1.0 mm^2 in-plane resolution, 5-mm slice thickness [6 total slices], TA = 6:09 min) were acquired.

2.9 | In vivo T_2 analysis

Several regions were segmented manually on matching axial slices of the T_2 maps for each method (2D PD-T2, MESE, and 3D FSE). Included regions of interest were the frontal white matter (64 total pixels), inferior longitudinal fasciculus (20), cortical gray matter (21), corticospinal tract/internal capsule (16), putamen (56), globus pallidus (48), thalamus (48), and red nucleus (25). Comparison of methods was made using Bland-Altman analysis.[37,38] Differences of each method compared with MESE for all regions and subjects were computed and tested for normality using a one-sided Kolmogorov-Smirnov test. An acceptable range of tolerance between two measurements was defined as the T_2 mean SD of each tissue measurement for all MESE regions in all subjects. As measured in Section 3, the mean MESE SD was equal to 4 ms; consequently, by this definition, two methods agree within limits if the confidence interval (CI) range is less than or equal to 8 ms.

3 | RESULTS

3.1 | Constant echo train simulations

Simulations for the constant 32 echo train with flip angle of 120°, echo selections of 1 (S_1, effective TE [TE_{eff}] of 6 ms) and 16 (S_2, [TE_{eff}] = 96 ms), and nominal B_1^+ of 1.0 are shown in Figure 1B,C, with signal as a function of T_1 and T_2. The signal response at T_2 = 100 ms and T_1 = 1 s is illustrated in Figure 1A (as compared with a constant 180° train). These echoes were chosen to mimic the 2D PD-T2 contrasts (typically using echoes 1 and 9 in a 16-echo sequence, corresponding to TE_{eff} of 10 ms and 90 ms, respectively). Maximum echo signal variance (S_{nd}) across in vivo T_2s was calculated to be 0.58 with an average of 0.51 (measured between 30 and 100 ms at a constant T_1 of 1 s). The nearly constant T_1 variation illustrated by S_{nd} (Figure 1E) indicates mapping using the constant 32-echo sequence with 120° flip angle is practically T_1 invariant. Consequently, the assumption of a constant T_1 in T_2 quantification to reduce the number of variables is valid. Due to the T_1 invariance, further reduced TR cases (32 echoes with TR of 0.5 s and 16 echoes with minimal TR of 0.2 s) were explored but did not provide sufficient SNR in phantom and in vivo experiments.

3.2 | Generic train simulations

The response and flip angles for a 3D-FSE sequence commonly used for T_2-weighted images with signal plateau at T_2 = 100 ms (P100) are shown in Figure 2. Figure 2A illustrates the signal response of three T_2 isochromats (50, 100, and 200 ms) to the P100 sequence and shows the flip angle evolution used to produce the signal. Further analysis of the spread of different T_2 decays for a T_2 range of 20 to 200 ms is shown in Figure 2B (constant T_1), and T_1 decays (range of 0.6 to 1.6 s, constant T_2) in Figure 2C. Because the spread of response based on individual T_2 isochromats in Figure 2B is greatest following the plateau (echo number 53, TE_{eff} = 318 ms), it follows intuitively that this point would make an ideal second echo candidate for mapping T_2s in combination with an earlier echo in the train. Compared with the diverse variation of T_2 decays in Figure 2B, the amount of T_1 variation is noticeably constrained (Figure 2C), indicating a small variation in signal due to differences in T_1.

To investigate effects of adjusting the plateau, three variable flip angle sequences with plateaus occurring at 50 (P50), 100 (P100), and 200 ms (P200) were designed and simulated, and the decay curves are shown in Figure 3. As mentioned, P100 was used as the starting point, as it mimics the common T_2-weighted variable flip angle train used for clinical routine, while preliminary simulations showed an improved result in T_2 mapping when the plateau was optimized at a higher T_2 (P200). The P50 case was used to illustrate effects of using a lower T_2 plateau. The response of T_2 species in the in vivo range of 30–100 ms is illustrated for each variable flip angle train (P200, 3A; P100, 3B; P50, 3C) and compared with the constant flip angle, 32-echo case (Figure 3D). The required flip angle arrays are shown in each as the dotted line on the secondary *y*-axis. In the

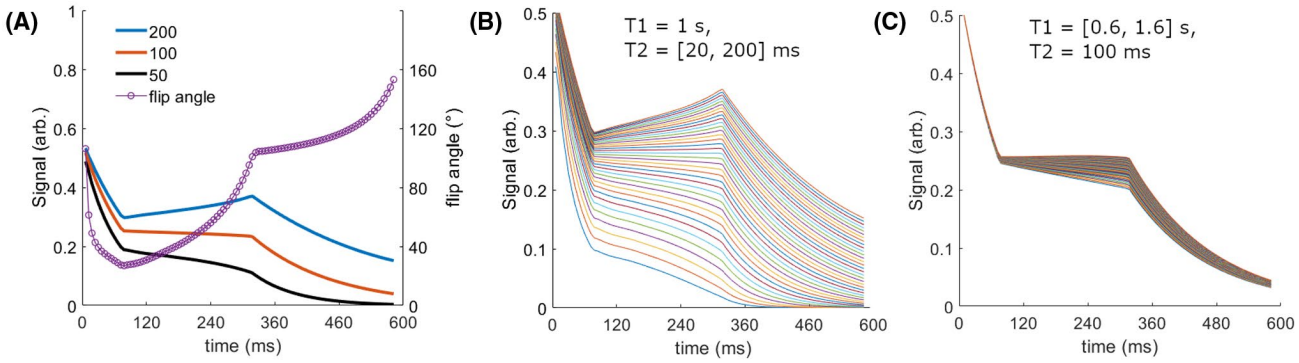

FIGURE 2 (A) Response at $T_2 = 200$ ms (blue), $T_2 = 100$ ms (orange), and $T_2 = 50$ ms (black) to the 96-echo flip angle evolution optimized for 100 ms (P100) prescribed in purple (secondary *y*-axis). B_1^+ and T_1 were held constant for this illustration with values of 1.0 and 1.0 s, respectively. Note the long ramp with sustained $T_2 = 100$ ms signal. The variation of the response is shown with respect to T_2 (B) and T_1 (C), where each line shows a different T_2 (in the range of 20–200 ms) or T_1 (with range of 0.6 to 1.6 s) species. Echo spacing is 6 ms; therefore, 60 ms denotes 10 echoes

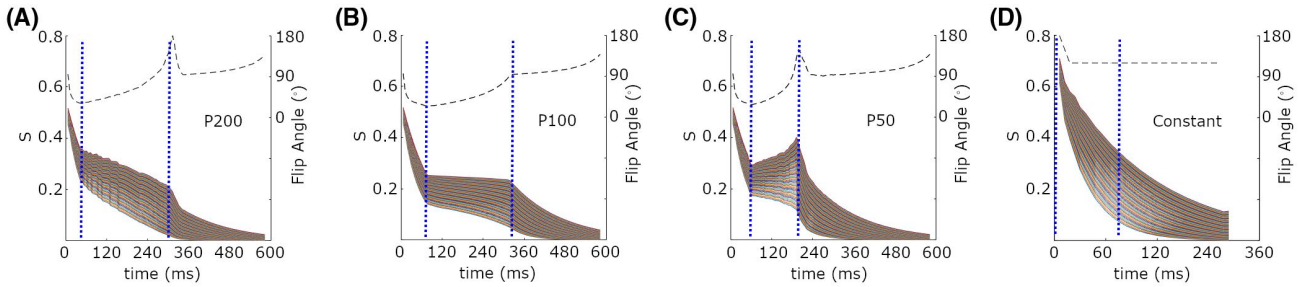

FIGURE 3 Spread of decay curves (multiple lines) for different T_2 values ranging from 20 to 200 ms for variable flip angle sequences. Sequences have been optimized to produce sustained signal at plateaus of $T_2 = 200$ ms (P200) (A), $T_2 = 100$ ms (P100) (B), and $T_2 = 50$ ms (P50) (C). The decay of the constant case is shown in (D). Vertical bars indicate the location of the chosen, optimized echoes for the T_2 mapping experiment. The flip angle train is shown as a dashed line at the top, corresponding to the secondary *y*-axis. All experiments used an echo spacing of 6 ms, with a total of 96 echoes (A-C) and 32 echoes (D)

case of P50, larger flip angles are needed earlier in the evolution to maintain the plateau due to the more rapid transverse decay of the $T_2 = 50$ ms isochromat in comparison to species with slower relaxation rates. There is substantial T_2 variation in all sequences, indicating that T_2 mapping utility is possible with variable trains, with the most spreading occurring for the P50 case.

Sequence evaluation and calculation of optimal TEs through S_p and oT2 was performed (Figure 4), and S_d, S_{nd}, and S_p for the optimal TEs are shown in Figure 4A–C. Although there is some T_1 variation at higher T_2 values (curvature of the plane in the T_1 direction in S_{nd}), there remains a very small variance of signal due to T_1 contributions in the in vivo range (<3% for P200). The largest signal difference occurs for P200 (4A), with a gradual decline in difference toward higher T_2 values. Although P50 shows some ability to distinguish T_2 values < 40 ms, S_p is close to zero around the T_2 values of interest ($T_2 = 60$ ms), and therefore should not perform as well as P100 or P200. P100 varies similarly to P200, with a reduced T_2 mapping capacity due to lower available contrast.

Analysis of oT2 (echo selection) resulted in optimized echoes in each case occurring near the beginning and before the end of the plateau (Figure 4D–F). Consequently, an earlier echo is prescribed for S_2 (33, $TE_{eff} = 198$ ms) in P50 versus S_2 for the P200 case (echo 49, $TE_{eff} = 294$). Optimal TE_{eff}s are shown as coordinates in the format (TE_{eff}PD, TE_{eff}T2). There is a considerable amount of variation in the P50 plot (Figure 4D) and a relative singular peak for optimal TEs, while more flexibility in TE selection is afforded with P100 and P200 (i.e., similar results can be achieved at several combinations due to the elongated maximum). Note that the optimal TEs in Figure 4D–F were used to produce the signal parameter maps in Figure 4A–C.

Evaluation of signal parameters in terms of T_2 and B_1^+ space using an expected B_1^+ range of 0.7 to 1.25 (where nominal $B_1^+ = 1.0$) and a constant T_1 of 1 s (Supporting Information Figure S1) resulted in significant variation in both T_2 and B_1^+ directions. This is contrasted to measured signal parameters in T_2 and T_1 space (Figure 4), where variation was constrained primarily to T_2, indicating a

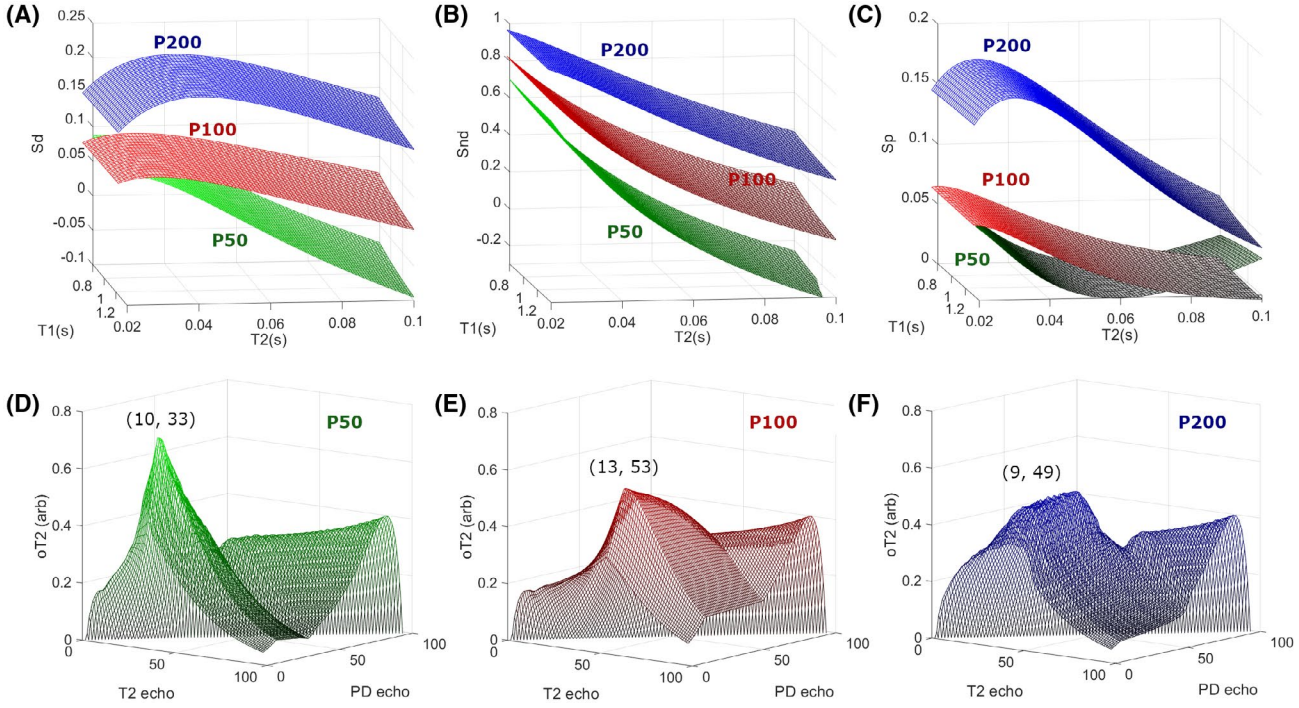

FIGURE 4 Signal difference (S_d) (A), normalized difference (S_{nd}) (B), and T_2 mapping performance (S_p) (C) for the three investigated variable trains. The greatest signal difference occurs in the P200 case (highest plane in [A]) showing the greatest available SNR after signal difference. The T_2 variation shown in S_{nd} is greatest for P50 (largest curvature in T_2 direction in [B]). C, S_p shows the best potential for accurate mapping occurs for the P200 sequence (a combination of T_2 variation and SNR). D-F, Optimized TEs using the ETL × ETL matrix approach for P50, P100, and P200. The coordinates of the peak of the optimization (oT2) are shown in brackets (proton density [PD] echo, T_2 echo). All sequences used an echo spacing of 6 ms. Note that the oT2 parameter is in arbitrary units

need to take both T_2 and B_1^+ into account when performing fitting using an acquired B_1^+ map. P200 showed a signal variation of 0.1 (T_2 = 100 ms, B_1 = 0.7) to 0.95 (T_2 = 30 ms, B_1^+ = 1.25), with a similar shape to S_{nd} (Figure 4B) in the T_2 direction. P100 showed less variation (0 to 0.8) in T_2, while the P50 case produced similarly shaped S_{nd} (B_1^+) maps to the P50 case in Figure 4B, with the least amount of total variation of 0 to 0.6 in T_2. The S_p analysis indicated best performance should be expected for the P200 case, with the greatest available contrast and most variation in T_2 and B_1^+ directions.

3.3 | Phantom experiments

Results of experiments using the six-cylinder phantom are shown in Figure 5, with T_2 values recorded in Table 1. The SNR measurements quoted were measured using the first vial image (MESE T_2 = 82 ms), and contrast-to-noise ratio (CNR) used an average for all vials (corrected to voxel size). The constant train with 32 echoes (C32, 5C) and P200 (5F) compared the most favorably with the MESE T_2 maps, having percent differences of 2.2 and 1.3, respectively. As the TR for C32 was equivalent to the variable trains (1.4 s), the time for acquisition was three times longer due to a shorter ETL, making the C32 case less feasible for clinical studies. All phantom T_2 maps show more variation and noise compared with MESE. C16 (constant flip angle train with 16 echoes and TR = 0.2 s, not shown) and P50 (5D)—as predicted from the simulations—were the worst performers, with large deviations from MESE, and therefore were not included in the in vivo study. The SNR decreases of the variable echo trains from MESE and 2D PD-T2 are due to increased resolution in the slice direction and longer ETL. Note that C32 maintains SNR near the 2D cases using an ETL one third the length of the P200/P100/P50 cases. Individual vial CNR measurements showed a small decrease with increasing T_2, as expected (Supporting Information Figure S2 and Supporting Information Table S1), although a strong relationship between CNR and accuracy of estimated T_2 values was not present between the different T_2 vials. However, the overall average CNR did correlate with increased accuracy of T_2 value estimation, indicating that a threshold of about 200 is required for accurate T_2 prediction. All sequences with CNRs below 200 performed poorly (P100, 79; P50, 88; C16, 140).

Spherical phantom experiments measuring T_2 variation due to B_1^+ (Supporting Information Figure S1D–F), illustrated a relatively constant T_2 across the phantom (Supporting Information Figure S1F), with an average value

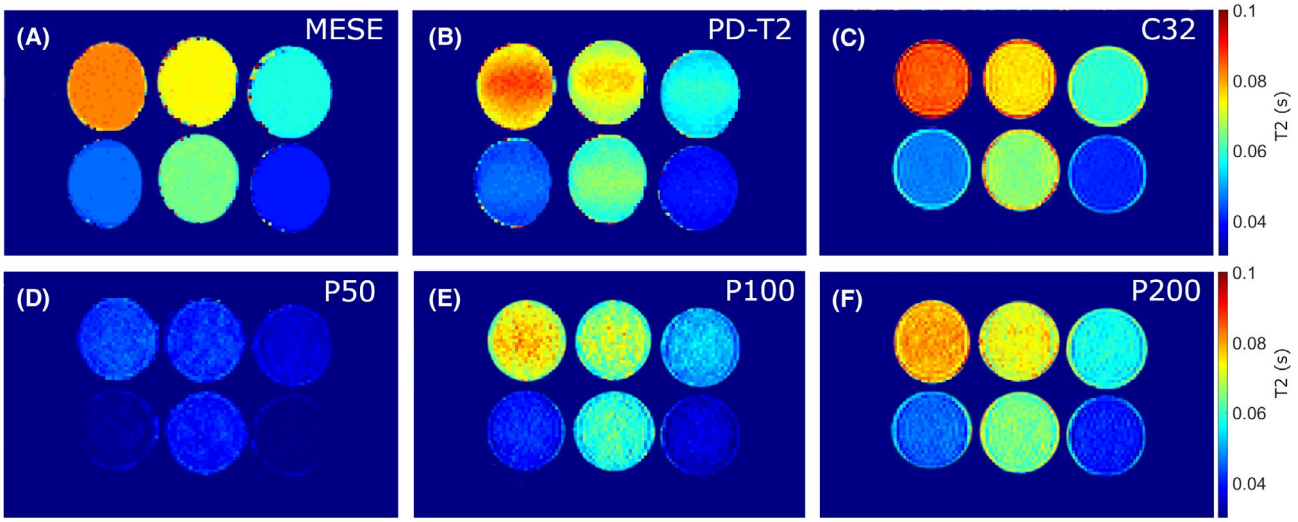

FIGURE 5 Phantom T_2 maps for 2D multi-echo spin-echo (MESE) (A) and 2D PD-T2 (B) experiments compared with the constant 32-echo train (C32) (C) and variable trains P50 (D), P100 (E), and P200 (F). The expected circular axial cuts are slightly elongated vertically in the MESE and PD-T2 cases due to thicker slices—illustrating the slight off-axis alignment of the phantom. Nominal phantom T_2 values that mimic in vivo brain tissues from the top left, clockwise, as measured from MESE, were 82.2, 73.9, 57.9, 40.0, 64.1, and 46.0 ms. The color bars are in seconds

TABLE 1 Phantom T_2 measurements for constant and variable flip angle trains

Train	Time (s)	SNR (PD-weighted)	SNR (T_2-weighted)	1[b]	2	3	4	5	6	Average CNR[c]	Diff from MESE (%)[d]
MESE	285	343	57[a]	82.2 ± 0.6	73.9 ± 0.5	57.9 ± 0.3	40.0 ± 0.0	64.1 ± 0.7	46.0 ± 0.1	418	–
PD-T2	182	328	178	82.8 ± 3.2	73.7 ± 2.9	57.5 ± 1.7	39.5 ± 1.1	63.8 ± 2.2	45.5 ± 1.2	336	0.7
C32	528	281	196	84.7 ± 1.4	75.1 ± 1.1	58.9 ± 0.8	41.0 ± 0.7	65.2 ± 0.1	47.1 ± 0.6	818	2.6
C16	150	71	58	86.3 ± 6.1	77.4 ± 5.7	63.4 ± 3.5	46.4 ± 2.0	68.6 ± 4.6	53.5 ± 2.2	140	10.4
P200	176	97	71	79.9 ± 2.3	72.4 ± 2.3	57.1 ± 1.9	40.2 ± 1.6	64.4 ± 2.4	45.7 ± 1.7	203	1.5
P100	175	58	80	75.4 ± 3.5	67.7 ± 3.8	52.4 ± 2.5	35.7 ± 1.5	60.4 ± 3.4	41.3 ± 1.7	79	9.5
P50	176	70	96	43.4 ± 1.5	41.4 ± 1.4	36.2 ± 1.0	29.5 ± 0.8	39.6 ± 1.3	31.5 ± 0.8	88	37.7

Abbreviation: CNR, contrast-to-noise ratio.

[a]SNR for MESE T_2 was measured on the 16th echo.

[b]Mean (in ms) ± SD.

[c]Corrected for voxel size.

[d]Difference from MESE was measured as the mean of percent differences for each cylinder.

of 135 ± 3.5 ms and a minimum value of 117 ms occurring at the periphery. B_1^+ varied between 0.76 and 1.26 (mean = 1.12, SD = 0.13). Reducing the measurement circle (excluding peripheral values) to a diameter of 18 cm resulted in a minimum T_2 of 126 ms. This indicates that extreme edge values of low B_1^+ may experience reduced T_2 values.

3.4 | In vivo experiments

Figure 6 shows demonstrative weighted images for P200 (PD image [Figure 6A] and T_2 image [Figure 6B]) and 2D PD-T2 (Figure 6C,D) used for T_2 mapping. The B_1^+ map is also included (Figure 6E) to display the measured B_1^+ variation across the brain. The 3D-PD image (Figure 6A) shows flatter PD tissue contrast than the 2D first-echo image (Figure 6C), and less signal from CSF. This is likely due to the more pronounced T_1 effects in 3D (TR = 1.4 s for 3D, TR = 7 s for PD-T2) as well as the removal of 2D incidental magnetization transfer effects.[39] T_2 maps for the two cases are shown in Figure 7 for two locations: (1) corticospinal tract and deep gray matter (Figure 7A,B) and (2) cortical gray matter, cerebellum, and superior longitudinal fasciculus (Figure 7C,D). A marked increase in resolution is apparent in the P200 case, with easier delineation in gray-matter folding and cerebellar structures. White-matter tracts including the corticospinal tract have less blurring and more definition in P200.

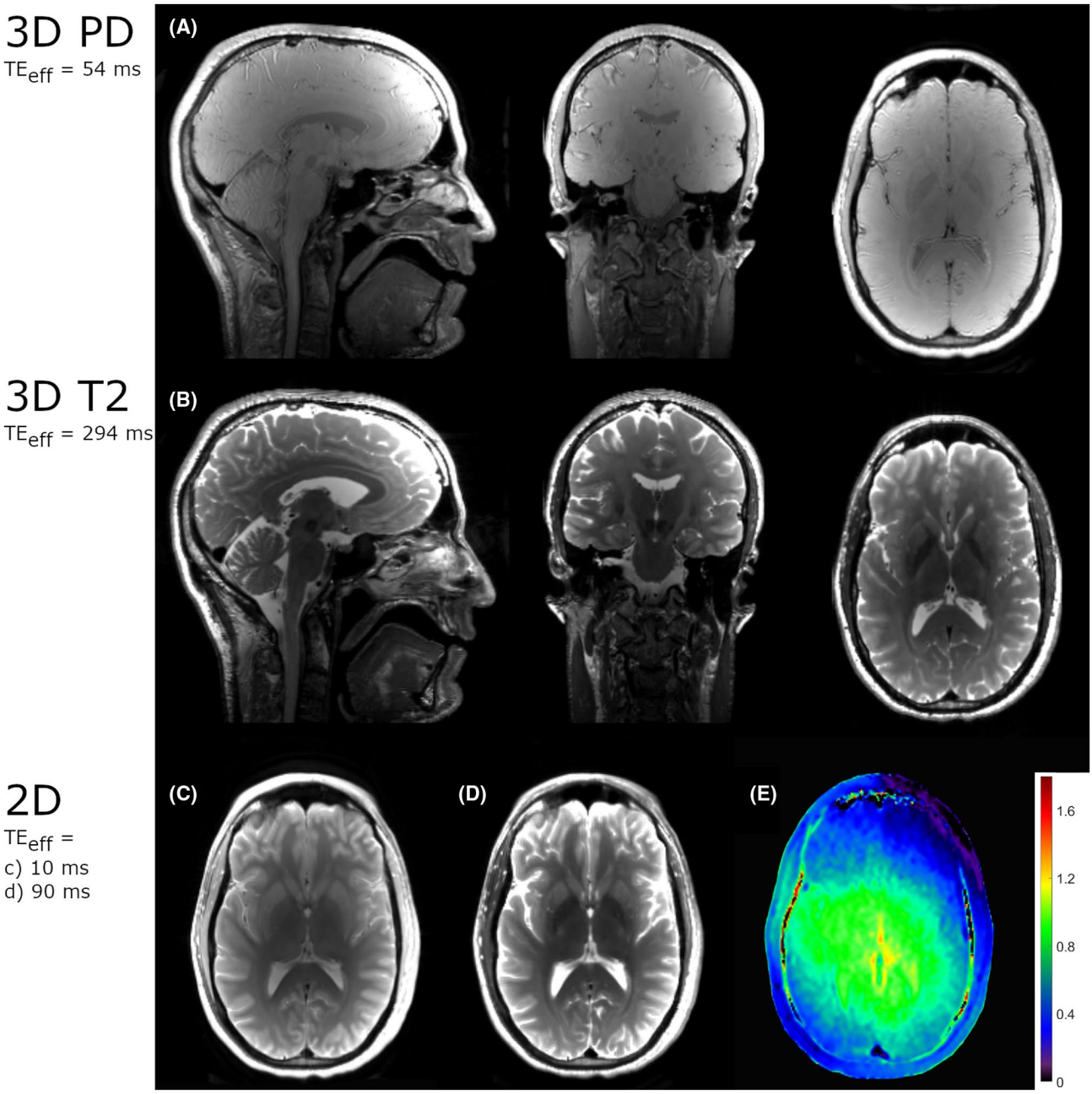

FIGURE 6 Raw (no smoothing or gradient removal) weighted images acquired for use in T_2 mapping. A, P200 3D sequence, PD echo (echo 9, $TE_{eff} = 54$ ms). B, T_2 echo of the 3D P200 sequence (echo 49, $TE_{eff} = 294$ ms). C, PD image for the dual-echo 2D sequence. D, T_2 image for the dual-echo 2D sequence. E, Normalized B_1^+ map

3.5 | In vivo T_2 analysis

Several regions were manually segmented (locations shown in Supporting Information Figure S3), and measured T_2 values are provided in Table 2. T_2 values were similar in each region when comparing between subjects using the same method (other than red nucleus, likely due to relatively small number of voxels), with the main variance occurring between methods. When comparing MESE to 3D methods, the largest deviations occurred in the frontal white matter and internal capsule. P100 consistently projected lower T_2 values than other methods and produced a noisier T_2 map as predicted by S_p.

Using Bland-Altman analysis, differences between MESE T_2 values for each region and the other methods were computed and tested for normality. The resultant plots illustrating the differences of the measurements are shown in Figure 8, with color coding based on the three different volunteers. PD-T2 has the smallest CI followed by P200 and P100. In each case, a negative bias occurs

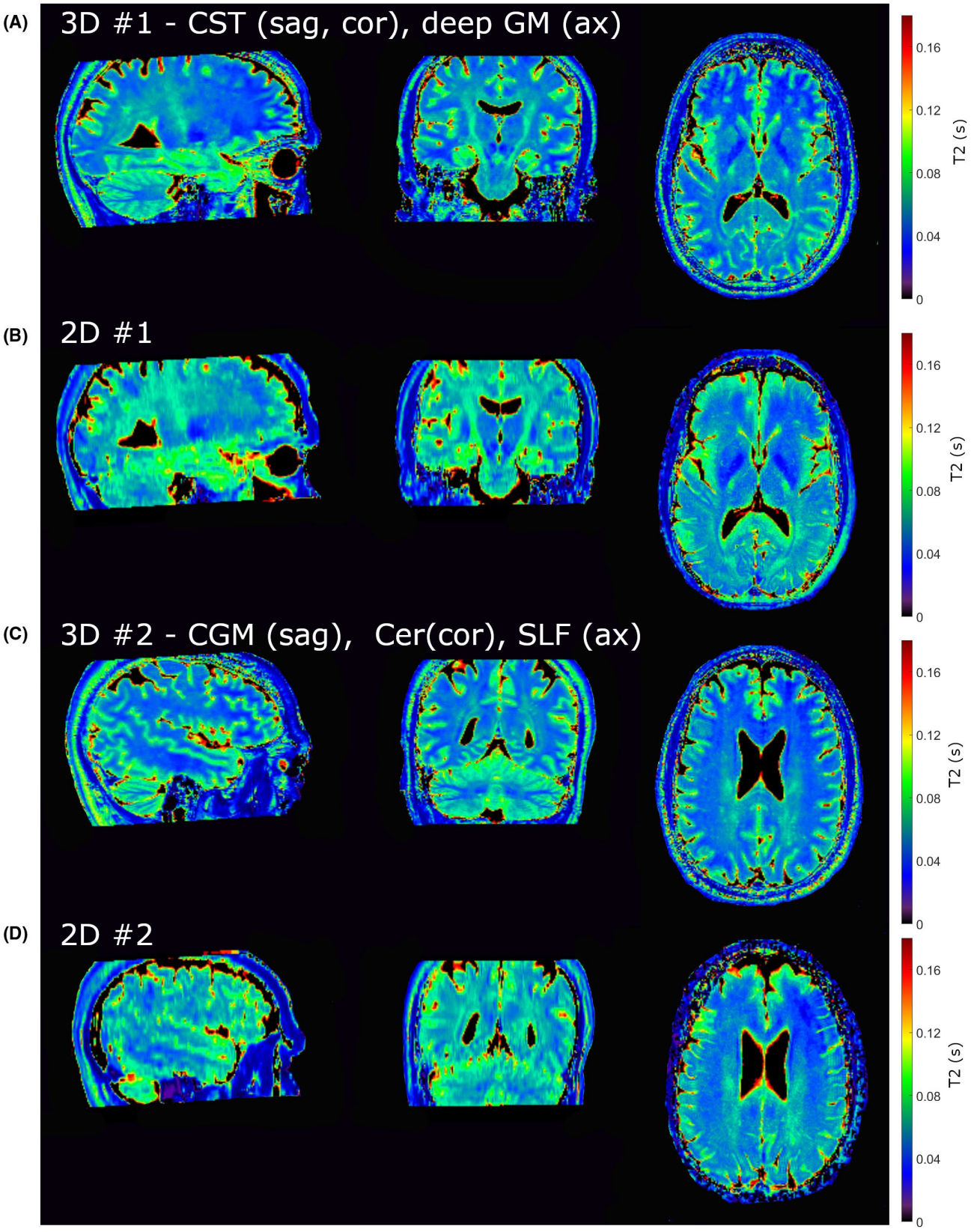

FIGURE 7 T_2 maps for the P200 variable flip angle case (A,C) and 2D PD-T2 (B,D), highlighting two locations. In #1 (A,B), the corticospinal tract (CST) is clearly visible on the 3D sagittal (sag) and coronal (cor) slices, while deep GM structures are illustrated in the axial view, particularly the internal capsule, thalamus, globus pallidus, and putamen. Location #2 features cortical GM folding (sag), a highly resolved cerebellum (Cer) in coronal 3D (C), and the tracts of the superior longitudinal fasciculus (SLF, axial). Of particular note is the three-fold improved slice resolution in the 3D sagittal and coronal reformats (see sag and cor #2 and structural nuance present in the CST in #1)

TABLE 2 T_2 values from 3 healthy subjects for 3D and 2D methods

	Time (s)	SNR PD	SNR T_2	FWM[a,b]	ILF	CGM	IC	Putamen	GP	Thalamus	RN	Diff from MESE (%)
V1												
MESE	396	180	65.0[c]	59.5 ± 1.2	73.8 ± 4.3	73.9 ± 3.0	85.0 ± 11	64.5 ± 4.1	50.4 ± 1.8	63.3 ± 2.7	51.6 ± 1.7	
PD-T2	238	155	73.8	57.4 ± 2.0	73.1 ± 3.5	74.0 ± 3.7	82.5 ± 3.7	61.5 ± 2.0	47.2 ± 2.6	60.1 ± 3.1	48.7 ± 3.0	3.7
P200	646	95.5	114	54.5 ± 1.3	73.6 ± 3.3	74.6 ± 4.2	79.4 ± 3.8	63.1 ± 2.6	48.6 ± 2.2	61.1 ± 2.0	49.8 ± 2.5	3.6
P100	646	56.5	43.9	49.4 ± 2.5	73.0 ± 5.3	72.6 ± 4.7	72.5 ± 3.0	62.7 ± 3.8	49.6 ± 2.4	62.7 ± 2.4	47.8 ± 3.1	5.9
V2												
MESE	396	203	79.0[c]	58.5 ± 1.5	74.6 ± 3.8	75.6 ± 3.9	81.4 ± 9.7	62.6 ± 3.5	52.0 ± 2.2	63.6 ± 3.0	–[d]	
PD-T2	238	175	91.0	55.6 ± 2.4	70.0 ± 2.7	74.0 ± 3.6	80.3 ± 5.6	62.3 ± 3.2	48.8 ± 3.6	61.7 ± 3.8	50.3 ± 3.5	3.5
P200	646	43.0	52.3	55.1 ± 2.6	72.0 ± 2.2	73.0 ± 4.7	78.9 ± 2.8	62.2 ± 3.4	51.6 ± 2.1	65.6 ± 2.0	61.1 ± 1.7	2.9
P100	646	33.8	37.2	49.4 ± 2.2	71.9 ± 2.5	73.8 ± 0.9	74.3 ± 1.9	61.0 ± 3.3	50.2 ± 3.3	62.1 ± 1.8	52.4 ± 3.0	5.5
V3												
MESE	396	212	78.9[c]	56.4 ± 2.7	71.0 ± 4.0	70.5 ± 2.8	81.9 ± 13	63.4 ± 3.6	46.9 ± 2.3	63.3 ± 1.8	53.4 ± 1.9	
PD-T2	238	132	91.6	55.6 ± 2.8	73.3 ± 3.4	72.6 ± 3.0	82.3 ± 6.1	59.8 ± 3.0	47.6 ± 5.7	62.6 ± 4.0	50.3 ± 5.2	2.8
P200	646	78.1	76.2	52.8 ± 2.7	70.5 ± 2.9	72.3 ± 3.2	76.3 ± 3.1	62.5 ± 2.7	49.8 ± 3.3	62.5 ± 2.7	53.1 ± 3.7	3.2
P100	646	62.9	73.4	45.1 ± 2.1	67.2 ± 1.9	82.1 ± 7.4	74.3 ± 4.7	57.2 ± 2.6	47.2 ± 3.4	59.0 ± 2.5	47.7 ± 3.6	9.9

[a]Manual segmentation locations are as follows with region-of-interest pixel counts in brackets: FWM, frontal white matter (64); ILF, inferior longitudinal fasciculus (20); CGM, cortical gray matter (21); IC, corticospinal tract/internal capsule (16); putamen (56); GP, globus pallidus (48); thalamus (48); and RN, red nucleus (25).

[b]Mean value (in ms) ± SD.

[c]SNR for the MESE T_2 case used the 16th echo image.

[d]Red nuclei were not included in the MESE slices for the second subject.

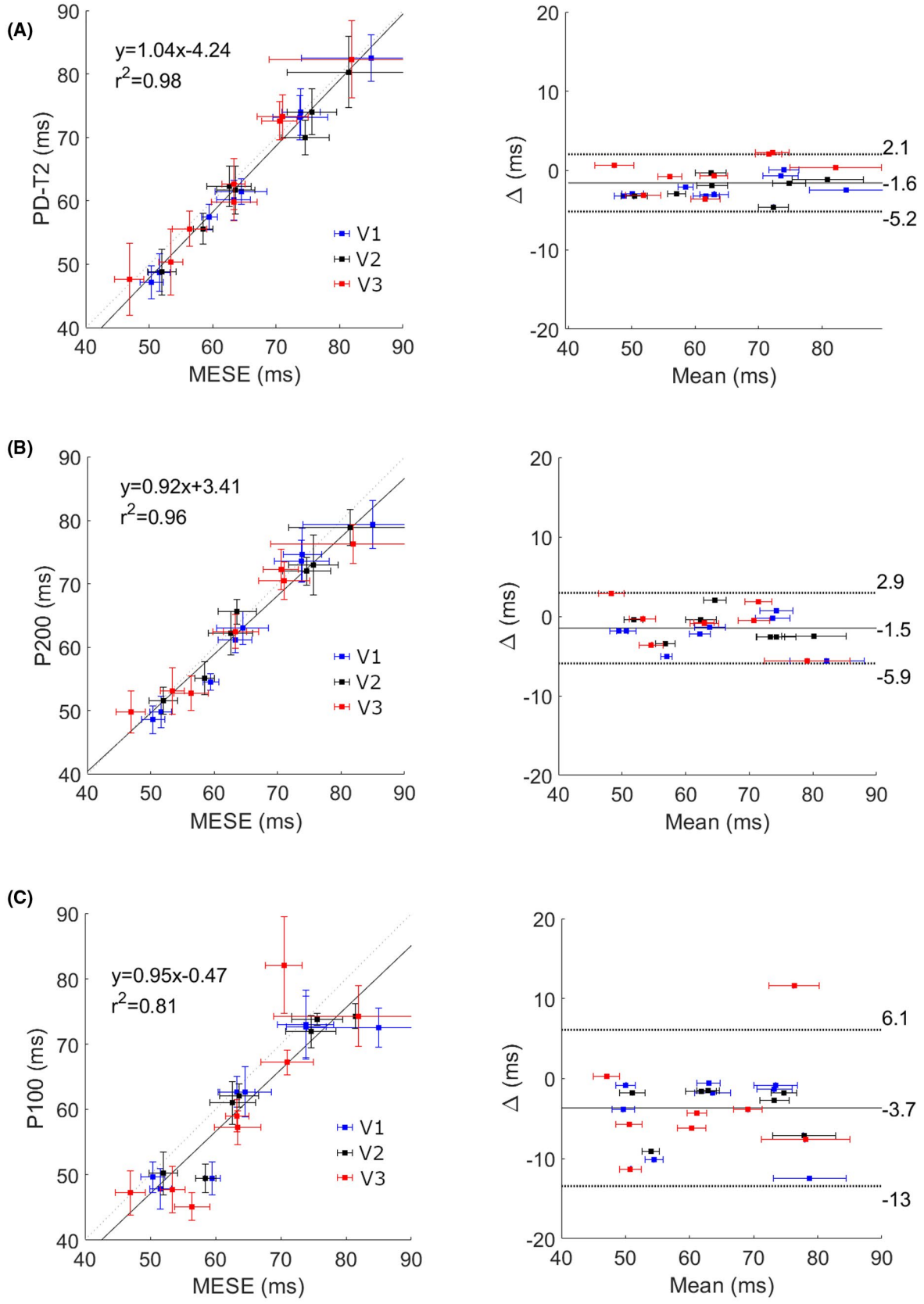

FIGURE 8 Correlation (left) and Bland-Altman (right) plots for comparison of MESE with 2D PD-T2 (A), P200 (B), and P100 (C) methods. Limits of agreement (confidence intervals) are shown in the Bland-Altman plots as dotted horizontal lines, with the mean bias as solid. Individual volunteers have been color-coded (volunteer 1, blue; volunteer 2, black; and volunteer 3, red)

ranging from 1.5 ms in the P200 case to 3.7 ms in P100, indicating underestimated T_2 values when compared with MESE. As expected, P100 is the poorest match for MESE, with CI ranging from –13 ms from the mean to +6.1 ms, and a total range of 19.1 ms, well beyond the defined acceptable value of 8 ms. P200 and PD-T2 are both within acceptable agreement, with CI ranges of 7.8 and 7.3 ms, respectively.

4 | DISCUSSION

A development of a dual-echo 3D T_2 mapping method with optimized flip angles is presented and compared with 2D PD-T2 and MESE standard methods. Simulations were used to compute signal response for optimization of flip angles and other sequence parameters as well as dictionary production for T_2 mapping. Three variable flip angle trains and a 32-echo constant flip angle case (reflecting 2D methods) were compared and verified in phantom measurements, and tissue T_2 values were compared with 2D methods using the variable trains. The standard 2D MESE measures for in vivo tissues were in agreement with past studies from our laboratory.[32]

The P200 variable flip angle train performed better than P100, as expected from simulations and phantom experiments, and was within the defined acceptable limits of agreement with MESE based on Bland-Altman analysis. Consequently, this allows higher spatial resolution and simplicity of modeling RF pulses, offering potential improvements over 2D methods. The PD-T2 method also showed a slight deviation from MESE values with an approximately 2-ms negative bias, similar to P200. Both methods use substantially fewer TEs for mapping compared with MESE (2 vs. 32) and likely contain similar errors in decay curve matching.

Although T_2 mapping provides a quantitative measure of tissue in pathology, clinical exams continue to rely on weighted images for diagnosis. High-resolution images with typical contrasts, in this case PD-weighted and T_2-weighted, were part of the design criteria for the 3D mapping sequence. Recent methods focusing more on quantitative imaging aspects, such as the stack of stars technique,[15] show promise in speeding up acquisition—the main drawback of the dual-echo 3D approach—while providing high-resolution 3D volumes with T_2-weighted images (~7 min vs. ~11 min for dual-echo 3D), although further comparison with previous methods and literature T_2 values is necessary. Additional gradient modules can also be introduced for faster sampling,[18] or can replace part or all of the typical SE readouts. For example, in a recent study,[40] 3D-FLASH readouts were used to determine quantitative measures in brain, although T_2 values are elevated 10%–15% from those presented in the 3D dual-echo case previously. Combination SE/GE sequences introduce complexities in modeling for dictionary values compared with the Bloch or EPG nonselective approaches; therefore, reference phantom values are required or machine learning techniques are used, as commonly employed in MR fingerprinting.[22,23] Furthermore, the 3D dual-echo approaches developed here are relatively T_1-invariant and substantial simplifications can be made when modeling signal evolution.

The acquisition of multiple volumes for quantification is subject to motion and can lead to erosion of resolution in the resultant T_2 map. As classification of tissue values is typically based on voxel averaging of segmented regions, T_2 reporting should not be greatly affected. It should be noted that using extended regions of interest for quantification does not necessarily degrade the gains of 3D methods—a finer region of interest (sharper edges including less of the surrounding tissues) can be delineated, resulting in less region-of-interest contamination and more accurate T_2 measures. Motion-correction techniques could alleviate the problem[41]; however, a combined dual-echo sequence—a true analogue of 2D PD-T2—would effectively remove interscan motion. The dual-contrast sequence could be designed to share echoes[42] to reduce TA while maintaining production of PD-weighted and T_2-weighted base images, with extension to multi-echo methods for further quantitative measures (such as T_1). Techniques to alleviate intrascan motion have recently been proposed for constant flip angle train FSE sequences[43] and will be investigated for variable flip angle trains in future work.

Limitations of our study include the use of healthy-tissue T_1 and T_2 ranges in the simulations (800–1400 ms and 40–90 ms, respectively) and the adjustment of flip angle arrays within the sequence source code. The T_1 and T_2 ranges used are insufficient to quantify the long T_2 times in CSF, although the focus of this study was the viability of variable flip angle trains using a T_2 range corresponding to healthy tissues. In clinical study, the expected T_2 range for the pathology should be considered. In terms of sequence programming, the modification of the flip angle array is the only requirement to enable these sequences and is possible using any scanner development software. However, some sites may not have access to the source code for sequences, making the implementation difficult. In these cases, researchers can test site-specific use of the T_2 variable flip angle train sequence (CUBE, VISTA, or SPACE) through manipulation of TE_{eff} for PD-weighted and T_2-weighted image production. Additionally, future work should include a robust discussion of the point-spread function effects on the selected echo trains. Although the results shown here have been compared with MESE experiments that

do not exhibit this problem, they are limited to the sequence parameters explored, and may not necessarily be extrapolated to variations in the sequence due to effects including the point-spread function.

Finally, while acquisition of images used for T_2 mapping is on the order of minutes, calculation of T_2 maps based on dictionary fitting using minimization typically takes several hours. Previous studies have reported computation times of 22–50 min for single-slice MESE experiments,[29] comparable to our study, whereas PD-T2 methods are on the order of 5 min/slice. While processing times are generally viewed as a nuisance to researchers, the applicability of T_2 mapping methods to clinical practice may hinge on the future ability to provide an efficient and accurate T_2 map calculation in line with base image acquisition on the scanner.

5 | CONCLUSIONS

The dual-echo 3D approach using variable flip angle trains is a viable T_2 mapping method based on simulated dictionary values while providing high-resolution PD-weighted and T_2-weighted base images. Optimization of the sequence parameters resulted in tissue T_2 values in brain in agreement with previous studies, indicating that the 3D approach can provide useful T_2 maps with superior anatomical detail in comparison to commonly used 2D methods.

ORCID

Jeff Snyder https://orcid.org/0000-0002-5043-2202
Kelly C. McPhee https://orcid.org/0000-0001-8239-4805

REFERENCES

1. Kitajima M, Hirai T, Shigematsu Y, et al. Comparison of 3D FLAIR, 2D FLAIR, and 2D T_2-weighted MR imaging of brain stem anatomy. *Am J Neuroradiol*. 2012;33:922-927.
2. Dodo T, Okada T, Yamamoto A, et al. T_1-weighted MR imaging of glioma at 3T: a comparative study of 3D MPRAGE vs. conventional 2D spin-echo imaging. *Clin Imaging*. 2016;40:1257-1261.
3. Bapst B, Amegnizin J-L, Vignaud A, et al. Post-contrast 3D T_1-weighted TSE MR sequences (SPACE, CUBE, VISTA/BRAINVIEW, isoFSE, 3D MVOX): technical aspects and clinical applications. *J Neuroradiol*. 2020;47:358-368.
4. Hennig J, Weigel M, Scheffler K. Calculation of flip angles for echo trains with predefined amplitudes with the extended phase graph (EPG)—algorithm: principles and applications to hyperecho and TRAPS sequences. *Magn Reson Med*. 2004;51:68-80.
5. Weigel M, Hennig J. Development and optimization of T_2 weighted methods with reduced RF power deposition (Hyperecho-TSE) for magnetic resonance imaging. *Z Med Phys*. 2008;18:151-161.
6. Hennig J. Multiecho imaging sequences with low refocusing flip angles. *J Magn Reson*. 1988;78:397-407.
7. Hennig J, Scheffler K. Hyperechoes. *Magn Reson Med*. 2001;46:6-12.
8. Hennig J, Scheffler K. Easy improvement of signal-to-noise in RARE-sequences with low refocusing flip angles. Rapid acquisition with relaxation enhancement. *Magn Reson Med*. 2000;44:983-985.
9. Hennig J, Nauerth A, Friedburg H. RARE imaging: a fast imaging method for clinical MR. *Magn Reson Med*. 1986;3:823-833.
10. Mugler JP. Optimized three-dimensional fast-spin-echo MRI. *J Magn Reson Imaging*. 2014;39:745-767.
11. Busse RF, Hariharan H, Vu A, Brittain JH. Fast spin echo sequences with very long echo trains: design of variable refocusing flip angle schedules and generation of clinical T2 contrast. *Magn Reson Med*. 2006;55:1030-1037.
12. McPhee KC, Wilman AH. T_2 quantification from only proton density and T_2-weighted MRI by modelling actual refocusing angles. *NeuroImage*. 2015;118:642-650.
13. Majumdar S, Orphanoudakis SC, Gmitro A, O'Donnell M, Gore JC. Errors in the measurements of T_2 using multiple-echo MRI techniques. I. Effects of radiofrequency pulse imperfections. *Magn Reson Med*. 1986;3:397-417.
14. Uddin MN, Marc Lebel R, Wilman AH. Transverse relaxometry with reduced echo train lengths via stimulated echo compensation. *Magn Reson Med*. 2013;70:1340-1346.
15. Keerthivasan MB, Saranathan M, Johnson K, et al. An efficient 3D stack-of-stars turbo spin echo pulse sequence for simultaneous T_2-weighted imaging and T_2 mapping. *Magn Reson Med*. 2019;82:326-341.
16. Zi R, Zhu D, Qin Q. Quantitative T_2 mapping using accelerated 3D stack-of-spiral gradient echo readout. *Magn Reson Imaging*. 2020;73:138-147.
17. Benkert T, Mugler JP, Rigie DS, Sodickson DK, Chandarana H, Block KT. Hybrid T_2- and T_1-weighted radial acquisition for free-breathing abdominal examination. *Magn Reson Med*. 2018;80:1935-1948.
18. Prasloski T, Rauscher A, MacKay AL, et al. Rapid whole cerebrum myelin water imaging using a 3D GRASE sequence. *NeuroImage*. 2012;63:533-539.
19. Weidlich D, Schlaeger S, Kooijman H, et al. T_2 mapping with magnetization-prepared 3D TSE based on a modified BIR-4 T_2 preparation. *NMR Biomed*. 2017;30:e3773.
20. Ma D, Gulani V, Seiberlich N, et al. Magnetic resonance fingerprinting. *Nature*. 2013;495:187-192.
21. European Society of Radiology (ESR). Magnetic resonance fingerprinting—a promising new approach to obtain standardized imaging biomarkers from MRI. *Insights Imaging*. 2015;6:163-165.
22. Bipin Mehta B, Coppo S, Frances McGivney D, et al. Magnetic resonance fingerprinting: a technical review. *Magn Reson Med*. 2019;81:25-46.
23. Chen Y, Fang Z, Hung SC, Chang WT, Shen D, Lin W. High-resolution 3D MR fingerprinting using parallel imaging and deep learning. *NeuroImage*. 2020;206:116329.
24. Ben-Eliezer N, Sodickson DK, Block KT. Rapid and accurate T_2 mapping from multi-spin-echo data using bloch-simulation-based reconstruction. *Magn Reson Med*. 2015;73:809-817.
25. Weigel M. Extended phase graphs: dephasing, RF pulses, and echoes—pure and simple. *J Magn Reson Imaging*. 2015;41:266-295.

26. Lebel RM, Wilman AH. Transverse relaxometry with stimulated echo compensation. *Magn Reson Med*. 2010;64:1005-1014.
27. Huang C, Bilgin A, Barr T, Altbach MI. T_2 relaxometry with indirect echo compensation from highly undersampled data. *Magn Reson Med*. 2013;70:1026-1037.
28. Pauly J, Nishimura D, Macovski A, Le RP. Parameter relations for the Shinnar-Le Roux selective excitation pulse design algorithm. *IEEE Trans Med Imaging*. 1991;10:53-65.
29. McPhee KC, Wilman AH. Transverse relaxation and flip angle mapping: evaluation of simultaneous and independent methods using multiple spin echoes. *Magn Reson Med*. 2017;77:2057-2065.
30. Weigel M, Hennig J. Contrast behavior and relaxation effects of conventional and hyperecho-turbo spin echo sequences at 1.5 and 3 T. *Magn Reson Med*. 2006;55:826-835.
31. Alsop DC. The sensitivity of low flip angle RARE imaging. *Magn Reson Med*. 1997;37:176-184.
32. McPhee KC, Wilman AH. T_1 and T_2 quantification from standard turbo spin echo images. *Magn Reson Med*. 2019;81:2052-2063.
33. Sacolick LI, Wiesinger F, Hancu I, Vogel MW. *B*1 mapping by Bloch-Siegert shift. *Magn Reson Med*. 2010;63:1315-1322.
34. Jenkinson M, Smith S. A global optimisation method for robust affine registration of brain images. *Med Image Anal*. 2001;5:143-156.
35. Jenkinson M, Bannister P, Brady M, Smith S. Improved optimization for the robust and accurate linear registration and motion correction of brain images. *NeuroImage*. 2002;17:825-841.
36. Greve DN, Fischl B. Accurate and robust brain image alignment using boundary-based registration. *NeuroImage*. 2009;48:63-72.
37. Martin Bland J, Altman DG. Statistical methods for assessing agreement between two methods of clinical measurement. *Lancet*. 1986;327:307-310.
38. Giavarina D. Understanding Bland Altman analysis. *Biochem Medica*. 2015;25:141-151.
39. Chang Y, Bae SJ, Lee YJ, et al. Incidental magnetization transfer effects in multislice brain MRI at 3.0T. *J Magn Reson Imaging*. 2007;25:862-865.
40. Ma S, Wang N, Fan Z, et al. Three-dimensional whole-brain simultaneous T_1, T_2, and T_1 ρ quantification using MR Multitasking: method and initial clinical experience in tissue characterization of multiple sclerosis. *Magn Reson Med*. 2021;85:1938-1952.
41. Zaitsev M, Dold C, Sakas G, Hennig J, Speck O. Magnetic resonance imaging of freely moving objects: prospective real-time motion correction using an external optical motion tracking system. *NeuroImage*. 2006;31:1038-1050.
42. Johnson BA, Fram EK, Drayer BP, Dean BL, Keller PJ, Jacobowitz R. Evaluation of shared-view acquisition using repeated echoes (SHARE): a dual-echo fast spin-echo MR technique. *Am J Neuroradiol*. 1994;15:667-673.
43. Gao X, Hucker P, Hennig J, Zaitsev M. Strategies to improve intra-train prospective motion correction for turbo spin-echo sequences with constant flip angles. *Magn Reson Med*. 2021;86:852-865.

SUPPORTING INFORMATION

Additional supporting information may be found in the online version of the article at the publisher's website.

FIGURE S1 Signal difference (S_d) (A), normalized difference (S_{nd}) (B), and T_2 mapping performance (S_p) (C) for the three investigated variable trains with a constant T_1 of 1 s, and ranges of $T_2 = [20, 100]$ ms and $B_1^+ = [0.7, 1.25]$. A large amount of variation is present in both the T_2 and B_1^+ directions (in contrast to nearly constant performance in the T_1 direction in Figure 4A–C). P200 shows the greatest available contrast (highest plane in A) and best mapping performance (C), followed by P100 and P50. Variation in the B_1^+ direction reinforces the need for B_1^+ maps when fitting decay curves. D-F, Spherical phantom tests of T_2 mapping performance with B_1^+ variation comparable to that in the human head. Proton density (PD) and T_2 images are illustrated in the split image in (D), with the B_1^+ map in (E) and resulting T_2 map in (F) for the P200 sequence. The mean T_2 was 135 ms, with SD = 3.4 ms, and a range of −13% to +5%. Extreme values occurred at the periphery.

FIGURE S2 Phantom experimental data plotting contrast-to-noise ratio (CNR) versus T_2, as measured in the multi-echo spin-echo (MESE) experiment. The size of the markers corresponds to the percent difference in T_2 value as compared with MESE

FIGURE S3 Voxel locations as denoted on volunteer T_2 maps for the eight regions. Abbreviations: FWM, frontal white matter; GM, gray matter; GP, globus pallidus; IC, internal capsule; ILF, inferior longitudinal fasciculus; Pu, putamen; RN, red nucleus; Th, thalamus

TABLE S1 Phantom T_2 CNR measurements for constant and variable flip angle trains

How to cite this article: Snyder J, McPhee KC, Wilman AH. T_2 quantification in brain using 3D fast spin-echo imaging with long echo trains. *Magn Reson Med*. 2022;87:2145–2160. doi:10.1002/mrm.29113